ICARUS 105, 282–297 (1993)

Pluto's Radius and Atmosphere: Results from the Entire 9 June 1988 Occultation Data Set

R. L. MILLIS, L. H. WASSERMAN, O. G. FRANZ, AND R. A. NYE

Lowell Observatory, Flagstaff, Arizona 86001

J. L. ELLIOT, E. W. DUNHAM,[1] A. S. BOSH, L. A. YOUNG, AND S. M. SLIVAN

Massachusetts Institute of Technology, Cambridge, Massachusetts 02139

A. C. GILMORE AND P. M. KILMARTIN

Mount John University Observatory and Department of Physics and Astronomy, University of Canterbury, Christchurch, New Zealand

W. H. ALLEN

Adams Lane Observatory, Blenheim, New Zealand

R. D. WATSON, S. W. DIETERS, K. M. HILL, A. B. GILES

University of Tasmania, Hobart, Tasmania

G. BLOW AND J. PRIESTLEY

Carter Observatory, Wellington, New Zealand

W. M. KISSLING

Applied Mathematics Division, Department of Scientific and Industrial Research, Wellington, New Zealand

W. S. G. WALKER, B. F. MARINO, AND D. G. DIX

Auckland Observatory, Auckland, New Zealand

A. A. PAGE AND J. E. ROSS

University of Queensland, St. Lucia, Queensland

H. P. AVEY, D. HICKEY, H. D. KENNEDY, K. A. MOTTRAM, G. MOYLAND, AND T. MURPHY

University of Southern Queensland, Toowoomba, Queensland

C. C. DAHN

U.S. Naval Observatory, Flagstaff Station, Flagstaff, Arizona 86002

AND

A. R. KLEMOLA

Lick Observatory, Board of Studies in Astronomy and Astrophysics, University of California at Santa Cruz, Santa Cruz, California 95064

Received March 10, 1993; revised August 5, 1993

[1] Now at NASA Ames Research Center, Moffett Field, CA.

0019-1035/93 $5.00

We have analyzed all photometric observations of the 9 June 1988 occultation of the star P8 by Pluto in order to derive the radius of Pluto and certain parameters of its atmosphere. Our analysis is based on a "haze" model; but where relevant, we also discuss the thermal gradient model. With either model, the occultation observations yield a diameter for the limb of Pluto that is significantly larger than that found from mutual event observations by D. J. Tholen and M. W. Buie (1989, *Bull. Am. Astron. Soc.* 21, 981–982), but is in good agreement with the value from E. F. Young (1992, Ph.D. thesis, Massachusetts Institute of Technology). For a clear atmosphere (i.e., the thermal gradient model), we find the radius of the solid surface of Pluto and, obviously, also of the limb, to be 1195 ± 5 km. If the haze model is correct, the solid surface of the planet falls below 1180 ± 5 km, but the radius of the visible limb would be in the haze layer between 1185 and 1200 km. The degree to which the structure of Pluto's atmosphere is globally homogeneous is also discussed.

I. INTRODUCTION

In the course of an extensive search for occultations of stars by Pluto, Mink and Klemola (1985) noted the high probability that one such event involving a 13th-magnitude star (identified as P8) would occur on 9 June 1988. Subsequent photometry showed the star to be somewhat brighter: $V = +12.8$ (Bosh *et al.* 1986). Astrometric measurements at Lick Observatory, the U.S. Naval Observatory's Flagstaff Station, and Lowell Observatory were combined to produce a refined predicted groundtrack for this event, which crossed the South Pacific, New Zealand, and Australia (Wasserman *et al.* 1988).

The occultation was observed photometrically at eight sites: three in New Zealand, four in Australia, and one—the Kuiper Airborne Observatory—over the ocean south of the Samoa Islands. Given that the occultation occurred gradually, it was immediately evident that Pluto has an atmosphere (IAU Circular 4611). While the existence of an atmosphere was expected (e.g., Trafton and Stern 1983, Cruikshank 1987), unequivocal evidence of Pluto's gaseous envelope had not previously been recorded and the amount of atmosphere present was uncertain by several orders of magnitude.

Observations from the KAO (Elliot *et al.* 1989 [hereafter ELL], Elliot and Young 1992) and from Hobart, Tasmania (Hubbard *et al.* 1988), have been discussed at length in the literature. Elliot *et al.*, in order to explain the shape of the KAO occultation lightcurve, postulated the existence of a haze layer in Pluto's lower atmosphere. Millis *et al.* (1988) reached a similar conclusion from a less thorough analysis of observations from near Charters Towers in northern Queensland. The observations from Hobart did not probe deeply into the planet's atmosphere and, hence, evidence of the proposed haze layer is not present in that lightcurve.

For this occultation, unlike previous ones involving other planets, the usual assumption that the atmosphere is thin compared to the radius of the planet is invalid (Hubbard *et al.* 1988, ELL). Consequently, the component of the star's motion perpendicular to the limb cannot be considered to be constant throughout the atmosphere and focussing due to the local curvature of the atmosphere must be considered. Also, the acceleration of gravity cannot be treated as a constant in the analysis. Subsequent to the Elliot *et al.* paper, Eshleman (1989) and Hubbard *et al.* (1990) suggested that the lightcurve feature attributed by ELL and Millis *et al.* (1988) to a haze layer alternatively could have been produced by a steep, near-surface temperature gradient.

Because all the above-mentioned analyses have been limited to small subsets of the total observational data base from the 9 June occultation, the authors were unable to draw firm general conclusions concerning the planetwide characteristics of Pluto's atmosphere. Furthermore, lacking a definitive global solution for the precise location of the occultation ground track (ELL did generate a preliminary ground track based on data from three sites), they could not specify exactly the location of the apparent chord across Pluto traced by P8 as seen from their particular observing site. Hence, the altitude in the atmosphere corresponding to any particular feature in the lightcurve was somewhat uncertain, and the accuracy of the models based on individual data sets was therefore limited. In this paper we attempt to overcome the above limitations by including the total data set in the analysis.

II. THE OBSERVATIONS

Prediction of the region of observability for this event was particularly difficult because (a) Pluto subtended only about 0.13 arcsec, (b) its image on the photographic plates used for astrometry was invariably unresolved from that of Charon, and (c) its motion across the sky included a periodic component of unknown amplitude about the barycenter of the planet–satellite system. The predicted boundaries of the ground track, based on the astrometry of Wasserman *et al.* (1988), are shown as dashed lines in Fig. 1. On the basis of the repeatability of the astrometry and experience, this predicted track location was believed to have an uncertainty of approximately one-third the width of the track. In making the prediction, Wasserman *et al.* assumed an airless planet having a radius of 1173 km, a radius of 606 km for Charon, and equal densities for the planet and satellite. The locations of the eight sites from which the 9 June occultation was observed are shown as filled squares in the figure. From north to south, the observing sites are a location near Charters Towers (Queensland, Australia), where a portable telescope from Lowell Observatory was located; the Kuiper Airborne

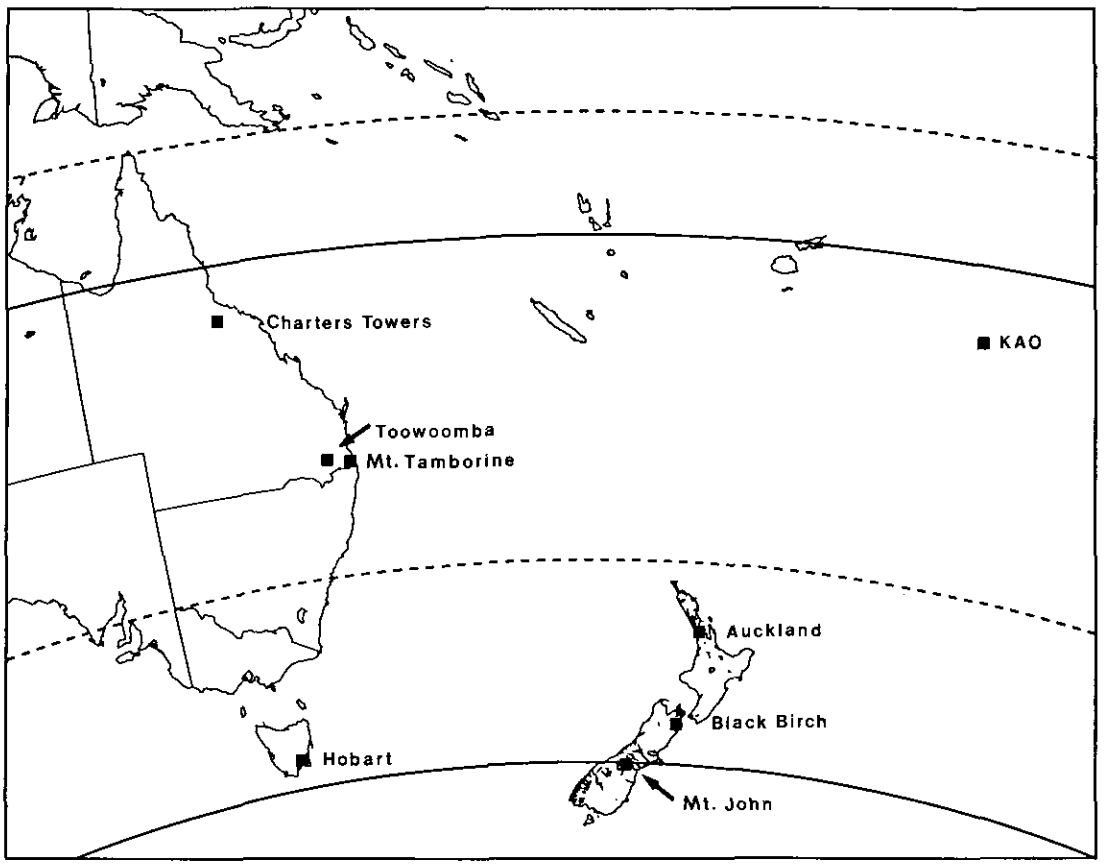

FIG. 1. Boundaries of the predicted (dashed lines) and observed (solid lines) ground tracks of the 9 June 1988 occultation of P8 by Pluto. The locations of observing sites are marked by filled squares.

Observatory; University of Southern Queensland (Toowoomba, Queensland, Australia); Mt. Tamborine Observatory, University of Queensland (St. Lucia, Queensland, Australia); Auckland Observatory (Auckland, New Zealand); Black Birch Observatory (near Blenheim, New Zealand); University of Tasmania Observatory (Hobart, Tasmania); and Mt. John Observatory (near Lake Tekapo, New Zealand). Planned observations at permanent observatories in the southern regions of the Australian mainland unfortunately were thwarted by clouds.

Coordinates of the observing sites and other relevant site-specific data are listed in Table I. Column 1 contains the site name; columns 2, 3, and 4 list the corresponding geographic latitude, geographic longitude, and altitude above sea level, respectively. Telescope aperture is listed in column 5, while the passband and/or detector type are given in column 6. The signal-to-noise ratio (S/N) of the data (i.e., the ratio of the average value of the pre- or postoccultation signal to the rms fluctuation of that signal when binned at a 1-sec integration time) is listed in the seventh column. The final two columns will be discussed later. Note that while the event was observed at three separate telescopes at Mt. John Observatory, those data have been averaged to produce one lightcurve with an improved S/N ratio.

The observed lightcurves are plotted in Fig. 2. Comparatively noisy curves from Toowoomba, Mt. Tamborine, and Auckland are plotted at one vertical scale; the others are plotted at a less compressed scale. The horizontal axis is the same for all the plots. All lightcurves have been normalized such that a brightness level of 1 corresponds to the combined signal of Pluto and P8, while a level of 0 corresponds to Pluto only. At Mt. John and the KAO, the relative contributions of Pluto and P8 were accurately measured sufficiently far in advance of the occultation that the two objects were still well separated. At other sites, the contribution of P8 to the total signal has been calculated based on Pluto's well-known rotational lightcurve (Tholen, personal communication), P8's measured brightness and color, and the passbands used for the observations. At the time of the occultation, the sub-Earth east longitude of Pluto was 308°, which corresponds to a rotational lightcurve phase well past maximum light on the descending branch of the lightcurve (see Buie and Tholen 1989).

The observations are quite heterogeneous, taken as

TABLE I
Observing Locations

Site name	Latitude	Longitude (East)	Altitude (m)	Aperture (m)	Passband[a]	S/N	Type	UTC at 23.6% Level
Charters Towers	−20°00′31″.30	+9^{h}45^{m}13^s.75	285	0.36	EMI 9789B	22.8	I	10 40 43.84 ± 0.88
					No filter		E	10 42 10.41 ± 1.57
KAO immersion	−20 25 06.00	−11 22 40.80	12500		Texas Instr.			
				0.9	CCD	74	I	10 36 35.55 ± 0.15
KAO emersion	−20 16 48.00	−11 22 59.20	12500		No filter		E	10 38 18.19 ± 0.15
Toowoomba	−27 47 58.00	+10 07 26.13	678	0.36	Silicon Pin Photo Diode	6.1	I	10 39 44.57 ± 0.6
					No filter		E	10 41 56.5 ± 0.5
Mt. Tamborine	−27 58 20.69	+10 12 51.18	530	0.32	*B*	3.8	I	10 39 42.8 ± 0.5
							E	10 40 52.1 ± 1.4
Auckland	−36 54 28.00	+11 39 06.53	80	0.50	EMI 9502	9.6	I	10 38 1.00
					No filter		E	10 40 5.69
Black Birch	−41 44 55.85	+11 35 12.87	1396	0.41	EMI 9813B	18.7	I	10 38 29.21 ± 0.9
					No filter			
Hobart	−42 50 57.30	+9 49 43.54	310	1.0	EMI 9858A	14.5	I	10 40 31.49 ± 1.4
					No filter		E	10 41 29.76 ± 2.5
Mt. John[b]	−43 59 14.70	+11 21 51.59	1029	0.61	*V*			
				0.61	*V*	21.7	—	10 39 19.62 ± 0.78
				1.0	*V*			

[a] *B* and *V* refer to the *UBV* system.
[b] Derived lightcurve is average of three observations.

they were with telescopes of different size, detectors of a variety of types, diverse passbands, and data recording equipment of varying degrees of sophistication. (The observations at Charters Towers, Toowoomba, and Mt. Tamborine, for example, were recorded in an analog mode and subsequently digitized for analysis.) Consequently, the large range in the photometric quality of the different data sets, which is readily apparent in Fig. 2, is not surprising. At one extreme, scintillation noise is virtually absent at the high altitude of the KAO, accounting, in part, for the high S/N ratio of those data compared with lightcurves from groundbased telescopes of similar aperture. The lightcurves from Mt. John, Hobart, and Charters Towers also are of relatively good quality, although at the latter site an unexplained apparent abrupt change in amplifier gain of nearly 10% occurred near mid-event. That transition was removed prior to plotting Fig. 2 and prior to further analysis by normalizing the immersion and emersion lightcurves separately. Sundry difficulties were encountered at other sites as well. At Black Birch, Pluto drifted to the edge of the photometer entrance aperture shortly after mid-occultation, thereby spoiling the emersion lightcurve. Electrical transients from the telescope drive electronics produced intermittent large spikes in the lightcurve from Auckland. The observations from Mt. Tamborine and Toowoomba are comparatively noisy, in part because of the small size of the telescopes used at those sites and, in part, presumably due to the characteristics of the detectors and photometer electronics. Even for the KAO, the uncertainty in the position of the aircraft during the observations is significantly larger than normal (see ELL).

It is evident upon inspection of Fig. 2 that the occultation occurred relatively slowly at most sites, although immersion at Mt. Tamborine appears to have been comparatively abrupt. Second, the rapid drop in brightness near the lower half of the lightcurve seen in the KAO data is clearly present also in the observations from Charters Towers and appears to be present in the Auckland data as well. We note, however, that the shape of the lightcurve at Auckland is quite different at emersion than at immersion. It is difficult to say with certainty whether the sharp step is present in the Toowoomba and Mt. Tamborine lightcurves, although we believe it is visible in the Toowoomba data. At Mt. John, Hobart, and Black Birch, the occultation was comparatively shallow and those lightcurves do not show this transition. Apparently the light from P8 did not, at those sites, probe to the level in the atmosphere where the sharp transition was produced—or did not sink deeply enough into that region to produce a detectable effect.

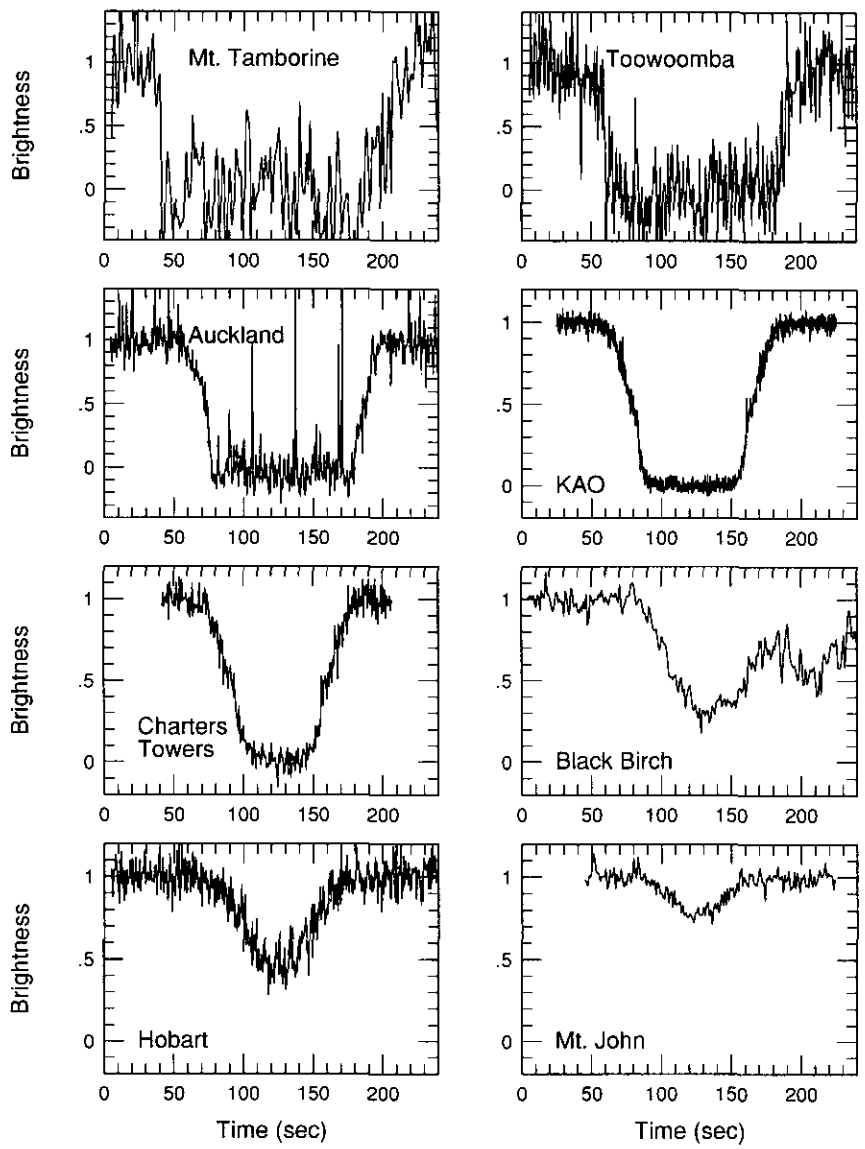

FIG. 2. Observations of the occultation of P8 by Pluto. The data have been normalized so that the preoccultation signal level corresponds to a brightness of 1 and the signal from Pluto alone corresponds to a brightness of 0. The data from Mt. Tamborine, Toowoomba, and Auckland are plotted at a more compressed vertical scale than the others because of their greater noise level.

III. ANALYSIS

Location of the Ground Track

The first step in the analysis was to specify as accurately as possible the location of the occultation ground track. Isothermal models were fitted by least squares to the data from sites where the occultation was relatively deep. Only those portions of the lightcurves above the step were included in the fit. Similarly, Gaussians were fitted to the shallower lightcurves from Hobart and Mt. John. These fitted functions then provided an objective way to determine the times at which the light from P8 was dimmed to a specific reference level at each site both on immersion and on emersion. In general, the fits to the data were quite good and certainly were adequate for this purpose. The reference level was chosen to be that corresponding to the minimum of the Mt. John lightcurve, i.e., a 23.6% reduction of the starlight. The times determined in this manner are listed in the last column of Table I. An I or E in the preceding column indicates immersion or emersion, respectively. The time listed for Mt. John is the time of minimum light.

The uncertainty in the quoted time at which the reference level was crossed depends on a number of factors. These include the timing accuracy of the observations themselves, the quality of the fit to the lightcurve, and

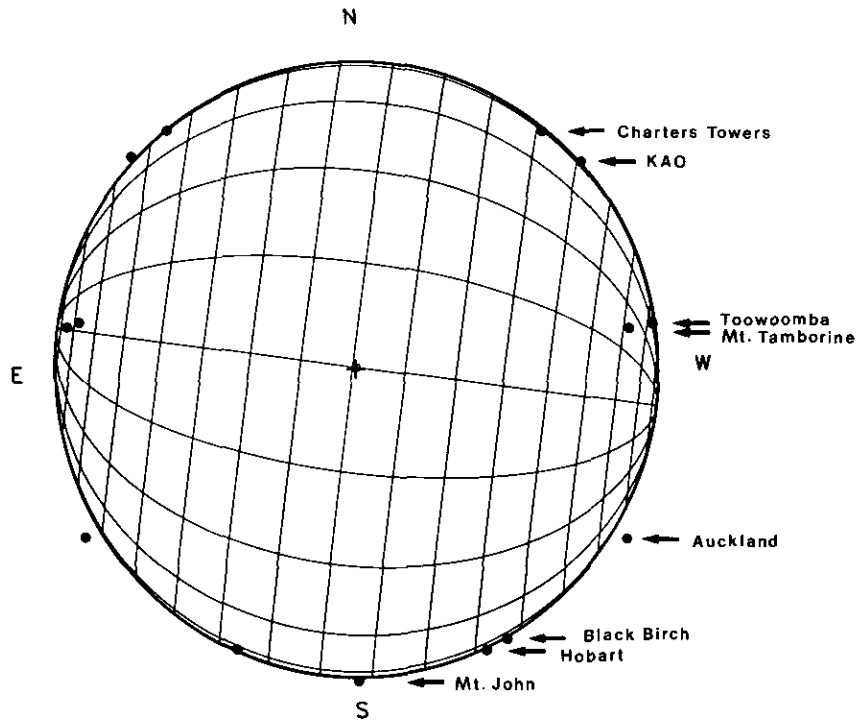

FIG. 3. A circle fitted by least squares to the observed points in Pluto's atmosphere corresponding to a 23.6% reduction of the light from P8. A latitude/longitude grid has been superimposed on the figure.

the accuracy to which the relative brightness of P8 and Pluto was known for each photometric system. Different factors dominated at different sites. Except for Toowoomba, Mt. Tamborine, and Auckland, the formal uncertainty as determined from the least-squares fit was dominant and is quoted in Table I as the uncertainty in the timing. For the Toowoomba data, we have quoted the reported uncertainty in the timing of the observations themselves, because it is significantly larger than the formal uncertainty of the least-squares fit, even taking into account the apparent uncertainty in the pre- and mid-event brightness levels. The quoted uncertainties for the Mt. Tamborine data are simply estimates. While the timing of the original stripchart recording of the lightcurve was better than our estimated errors suggest, the digitized version of the data used in our analysis did not reproduce the stripchart with complete fidelity. Finally, we have not quoted uncertainties for the Auckland data for reasons discussed below.

The times at which the various lightcurves crossed (or in the case of Mt. John, touched) the reference level were converted to points in the fundamental plane—the moving plane which passes through the center of the Earth and is perpendicular to the line connecting Pluto to the star (e.g., Smart 1960). Figure 3 shows the results of a least-squares fit of a circle to these data in which all observations were included with equal weight. (A coordinate grid is shown to indicate the location of Pluto's rotational axis relative to the regions of the atmosphere sampled by the observations.) An inconsistency between the points from Mt. Tamborine and Toowoomba, which fall along essentially the same chord, is immediately apparent. The difference between the two immersion points (on the right side of the figure), for example, corresponds to a timing difference of almost 7 sec. The chord from Auckland is also obviously too long to be well fitted by a circular profile. Because of the large spikes in the Auckland lightcurve and the existence of a large absolute timing error in those observations (the times from Auckland were shifted by 78 sec to obtain the degree of agreement shown in Fig. 3), we are concerned that substantial errors in the relative timing may also be present.

Because of these inconsistencies, several different least-squares solutions were computed, incorporating different weighting schemes and subsets of the data. The results are summarized in Table II, where we give, for a number of fitting schemes, the derived radius at the level corresponding to the minimum of the Mt. John lightcurve and the astrometric correction to declination and right ascension of Pluto (assuming that the star has no error in its position and is at 1950.0 RA $= 14^{h}49^{m}36^{s}.865$; Dec $= +00°57'19''.48$). Solution 1 includes all the observations weighted as the S/N ratio of the data; solution 2 includes the same data set weighted inversely as the S/N ratio of

TABLE II
Astrometric Solutions

Solution No.	Data used	Weighting	Radius at 23.6% diminution of starlight (km)	Correction to Dec of Pluto (")	Correction to RA of Pluto (sec)
1	All[a]	Signal-to-noise	1270.6 ± 7.4	0.34532 ± 0.00046	0.011015 ± 0.000031
2	All	Signal-to-noise squared	1277.8 ± 4.3	0.34536 ± 0.00029	0.011026 ± 0.000013
3	All	Equally	1252.2 ± 11.7	0.34479 ± 0.00082	0.010999 ± 0.000051
4	All	Timing errors	1268.9 ± 10.1	0.34558 ± 0.00069	0.011013 ± 0.000039
5	All	Timing error squared	1275.7 ± 8.2	0.34578 ± 0.00060	0.011026 ± 0.000018
6	S/N ≥ 10	Signal-to-noise	1277.0 ± 4.4	0.34526 ± 0.00019	0.011025 ± 0.000014
7	S/N ≥ 10	Signal-to-noise squared	1279.2 ± 4.1	0.34532 ± 0.00020	0.011029 ± 0.000009
8[b]	S/N ≥ 10	Equally	1274.4 ± 4.6	0.34514 ± 0.00018	0.011013 ± 0.000018

[a] Auckland was excluded in alternatives 1–5.
[b] Preferred solution.

the data squared; solution 3 includes all the data weighted equally; solution 4 includes all the data weighted inversely as their timing errors; and solution 5 includes all the data weighted inversely as their timing errors squared. Due to the problems with the Auckland observations described above, this data set was excluded from all solutions. Solutions 6, 7, and 8 use only the observations with a S/N ratio >10. From Table I, these are Charters Towers, KAO, Black Birch, Hobart, and Mt. John. Solution 6 has the same weighting as solution 1; solution 7 the same weighting as 2; and solution 8 the same weighting as 3. Restriction of the analysis to this subset of the data alone may be justified, in part, because of the better quality of these data. Moreover, the point of the calculation is to determine the centerline of the ground track so that the impact parameter for each site can be established. Observing sites near the edges of the track have greater leverage for this purpose than do those near the center. Note that the radii quoted in Table II are not particularly useful since they apply to an essentially arbitrary level in the atmosphere. The corrections to the RA and Dec determined from this solution establish the location of the ground track. The fitted values and errors for these two parameters are shown in Fig. 4 for all eight solutions. It is evident that, to within the errors, all the solutions are equivalent; they scatter only ±0.006 arcsec in declination and ±0.00002 sec of time in right ascension. Because Pluto's apparent motion across the star was nearly east–west, the uncertainty in right ascension translates into a timing error and is not important in computing the position of the ground track. The scatter in the declination correction corresponds to an uncertainty in the north–south position of the ground track centerline of only ±10 km. For purposes of the following analysis, we have adopted solution 8 as best for determining the location of the ground track for the June 9 occultation. The residuals corresponding to this solution are given in column 4 of Table III.

The impact of the uncertainty in the location of the KAO on the chosen solution was evaluated by recomputing the solution with the airplane shifted north and south of its nominal position by 7 and 15 km, respectively. In all cases the RA and DEC corrections did not change by more than the uncertainty quoted for solution 8.

The solid curves in Fig. 1 mark the "boundaries" (i.e., the distance from the centerline at which the star was dimmed by 23.6%) of the track corresponding to solution 8. Note that the actual track was shifted south relative to that predicted by Wasserman *et al.* (1988), by 0.037 arcsec

TABLE III
Residuals for Preferred Astrometric Solution

Site name	Immersion/ emersion	Weight	Residual (km)	Impact parameter (km)
Charters Towers	I	1.0	−13.1	985
	E	1.0	−7.5	
KAO	I	1.0	7.1	868
	E	1.0	15.1	
Toowoomba	I	0.0	−9.9	188
	E	0.0	−94.3	
Mount Tamborine	I	0.0	−110.5	168
	E	0.0	−47.2	
Auckland	I	0.0	61.5[a]	−687
	E	0.0	61.5[a]	
Black Birch	I	1.0	2.9	−1106
Hobart	I	1.0	3.7	−1153
	E	1.0	−15.6	
Mt. John	—	1.0	7.4	−1281

[a] Auckland was allowed to shift along its chord so the residuals are equal.

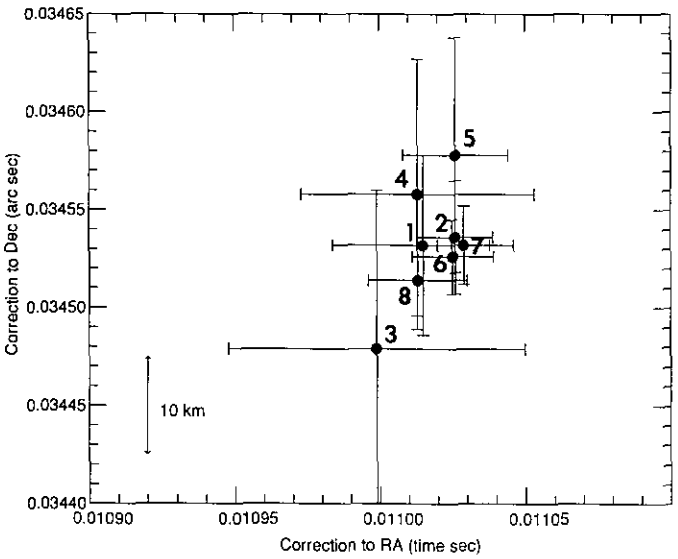

FIG. 4. Derived corrections to Pluto's ephemeris based on least-squares solutions using different weighting schemes and subsets of the data. See Table II.

(775 km), which is within the estimated uncertainty of the prediction. The difference in the width of the two tracks is in part due to projection effects and in part to the fact that the observed track pertains to a point high in Pluto's atmosphere, while the predicted track was based on the then-available estimate of the radius of the planet itself.

Determination of Pluto's Radius and Atmospheric Parameters

To reduce the noise, the data sets from all observatories except the KAO were averaged as shown in Table IV. The KAO data were employed in the analysis at their full 0.2-sec resolution. For each point on the lightcurve, the position of the center of Pluto on the fundamental plane (x, y) and the position of the observer (ξ, η) (e.g., Smart 1960) were computed. The position of the observer relative to the center of Pluto (and its shadow) as a function of time is then given by $H = (\xi - x)$ and $G = (\eta - y)$. A straight line was fitted by least squares to the derived set of (G, H) coordinates for each observing site. The coordinate frame was then rotated to (H', G') so that G' was effectively constant throughout the occultation.

In the rotated coordinate frame, each observation is a cut across the shadow of Pluto at constant impact parameter (G') and with the observed flux given as a function of (H'). For convenience in notation, hereafter we will refer to the G' coordinate as Y and the H' coordinate as X. Thus each observation is converted from flux as a function of time to flux as a function of X at constant impact parameter Y_{imp}. The derived impact parameters are given in the last column of Table III. This conversion eliminates the need to define a constant "perpendicular velocity" when, in fact, except for a site near the centerline, the apparent velocity of P8 perpendicular to Pluto's limb changes with time (see ELL). Note that the conversion of flux versus time to flux versus X requires an accurate ephemeris of Pluto relative to the occulted star. This ephemeris was produced by applying the corrections given for solution 8 in Table II to the JPL DE130 ephemeris. Because the KAO was moving throughout the occultation, it also was necessary to compute the aircraft's latitude and longitude at each point in time by interpolating between the positions at immersion and emersion (Table I). As ELL noted, the location of the aircraft had a

TABLE IV
Fits to Individual Observations

Observatory	λ_0	ν_0 ($\times 10^{-10}$)	Haze top (km)	$\tau = 1$ (km)	Haze scale height (km)	Shift (km)	Pluto + Star[a] (counts)	Pluto[b] (counts)	ΔT[c] (sec)	N[d]	σ[e]
Charters Towers immersion	21.87 ± 1.14	7.93 ± 0.64	1217.28 ± 1.62	1196.54 ± 2.24	31.0 ± 07.8	−12.40 ± 03.90	3482.38 ± 13.85	1258.50 ± 18.39	0.5	166	3.046×10^{-3}
Charters Towers emersion	24.29 ± 1.47	7.49 ± 0.71	1281.08 ± 1.57	1203.52 ± 1.89	23.6 ± 10.2	−3.30 ± 04.05	4318.34 ± 18.12	1835.21 ± 20.70	0.5	164	4.008×10^{-3}
KAO	21.42 ± 0.34	9.84 ± 0.02	1216.94 ± 0.46	1205.15 ± 0.53	29.3 ± 03.8	−6.55 ± 00.51	668.93 ± 00.86	126.35 ± 00.98	0.2	1000	1.271×10^{-3}
Toowoombe[f]	—	—	—	—	—	—	2814.1	2141.9	0.5	480	—
Mt. Tamborine[f]	—	—	—	—	—	—	514.4	403.9	0.5	600	—
Auckland[f]	—	—	—	—	—	—	1638.1	1206.2	0.5	480	—
Black Birch[g]	23.14 ± 1.12	9.96 ± 0.55	[h]	[h]	[h]	−21.75 ± 07.91	1341.81 ± 04.91	421.0	1.0	129	2.732×10^{-3}
Hobart[g]	21.67 ± 1.08	7.81 ± 1.00	[h]	[h]	[h]	18.96 ± 09.31	2201.24 ± 02.72	1625.5	0.5	480	7.199×10^{-3}
Mt. John[g]	25.13 ± 2.40	7.85 ± 0.59	[h]	[h]	[h]	−7.26 ± 14.10	997.01 ± 02.82	185.0	1.0	180	1.747×10^{-3}

[a] Pluto + star is the number of counts per integration of the combined light of Pluto and P8.
[b] Pluto is the number of counts per integration of the light from Pluto alone.
[c] ΔT is the integration time used in the analysis.
[d] N is the number of points.
[e] For each curve fit to the data, σ is the sum of $(O - C)^2$ divided by the number of points after the baselines of both the data and fit were normalized to 0 and 1.
[f] Toowoomba, Mt. Tamborine, and Auckland data were too noisy to fit for the atomospheric and haze parameters. For these curves, the Pluto + Star and Pluto alone baselines were determined by fitting a straight line to the unocculted and fully occulted regions of the lightcurves.
[g] The Black Birch, Hobart, and Mt. John lightcurves did not reach the Pluto alone baseline. For these lightcurves, this value was determined from data provided by the observers. Also, the Hobart and Mt. John curves did not reach the haze layer; the Black Birch curve may have just dipped into it.
[h] Haze parameters held constant at the KAO values.

systematic uncertainty throughout the occultation that could have been as large as 10–15 km.

The present analysis follows the Elliot and Young (1992) recent general treatment of a stellar occultation involving a planet with a spherically symmetric atmosphere. In their paper, the relevant equations are written in the most general case; i.e., they allow for the molecular weight to vary with altitude with power index, a, and for the temperature to vary with altitude with power index, b. For this analysis, we take both the molecular weight and the temperature to be constant. Thus, $a = b = 0$. The relevant equations are expanded in terms of a power series in $\delta = 1/\lambda$, where λ is defined below. For Pluto, terms of $O(\delta^2)$ are sufficiently small that they may be ignored (see Tables V or VI). Also, in the case of Pluto, under either the haze layer model or the thermal gradient model, the "far limb" contribution to the observed flux will be zero.

We have two coordinate systems. In the first, r measures distances radially away from the center of Pluto on the sky plane. In the second, ρ measures distances radially away from the center of the shadow of Pluto projected onto the fundamental plane. Then, as a function of r, the flux seen by the observer is given by

$$\phi(r) = \frac{e^{-\tau(r)}}{(1 + D\theta(r)/r)(1 + Dd\theta(r)/dr)}, \tag{1}$$

where D is the distance from the observer to Pluto, $\tau(r)$ and $\theta(r)$ are, respectively, the absorption (if any) and the bending along a ray which passes a distance r from Pluto. θ is the r derivative of the integral of the atmospheric refractivity along the ray path, while τ is the integral of the linear absorption coefficient along the ray path. ρ and r are related by the equation $\rho = r + D\theta(r)$.

Elliot and Young show that

$$\theta(r) = -\nu_0\sqrt{2\pi\lambda}e^{\lambda-\lambda_0}\left(1 - \frac{3}{8\lambda}\right) \tag{2}$$

and

$$\frac{d\theta(r)}{dr} = \frac{-\nu_0\sqrt{2\pi\lambda_0^3}}{r_0}\left(\frac{r_0}{r}\right)^{2.5}e^{\lambda-\lambda_0}\left(1 + \frac{1}{8\lambda}\right), \tag{3}$$

where r_0 is some arbitrarily chosen reference radius in the atmosphere, ν_0 is the refractivity of the atmosphere at that level, and λ is a function of r and is given by

$$\lambda = \frac{GM_p\mu m_{amu}}{kTr}. \tag{4}$$

In this equation, G is the gravitational constant, M_p is the mass of Pluto, μ is the (constant) mean molecular weight of the atmosphere, m_{amu} is the mass of one atomic unit, k is Boltzmann's constant, and T is the (constant) atmospheric temperature. The value of λ at $r = r_0$ is written as λ_0.

The lower part of the atmosphere must have either a haze layer (ELL) or a sharp thermal gradient (Hubbard *et al.* 1988, Eshleman 1989) to account for the sharp drop in the observed lightcurves. Again, we follow ELL and choose a haze layer characterized by a haze-top level (above which $\tau = 0$) at $r = r_1$ and a level at which $\tau = 1$ at $r = r_2$. The scale height of the haze at r_2, $H_{\tau 2}$, is a free parameter in the model. (The haze scale height is assumed to have the same dependence on altitude as does the atmospheric scale height, $1/r^2$, but our results are not strongly dependent on this assumption.) With these assumptions, Elliot and Young (1992) find that[2]

$$\tau(r) = \begin{cases} 0 & r > r_1 \\ \exp\left[-\dfrac{(r - r_2)}{H_{\tau 2}(r/r_2)}\right]\left(\dfrac{r}{r_2}\right)^{3/2}\dfrac{\mathrm{erf}[\sqrt{r_2^2(r_1^2 - r^2)/(2H_{\tau 2}r^3)}]\,S_1}{\mathrm{erf}[\sqrt{(r_1^2 - r_2^2)/(2H_{\tau 2}r_2)}]\,S_2} & r \le r_1 \end{cases} \tag{5}$$

where $S_1 \sim [1 + (9H_{\tau 2}r/8r_2^2)]$ and $S_2 \sim [1 + (9H_{\tau 2}/8r_2)]$. Our task then was to find the values of eight unknowns which fall into three groups. The first group, λ_0 and ν_0, defines the shape of the lightcurve above the haze layer. The second group, r_1, r_2, and $H_{\tau 2}$, defines the properties of the postulated haze layer. The third group of unknowns is observatory-specific and consists of the baselines for the lightcurves and a timing error at each observing site. The baselines are the counts per integration of Pluto + Star and of Pluto alone. The timing error is expressed as an error in X in kilometers (and can be expressed as a time by dividing by the shadow velocity).

The analysis proceeded as follows: First, we chose the reference level r_0 as 1250 km. Then, in order to minimize the complexity of the global fit to the data, each observatory's lightcurve was fitted independently in order to determine the baselines. This fit (eight parameters—two atmospheric, three haze, two baselines, and X shift) was

[2] This equation is taken from an earlier version of their paper where $\tau(r)$ is expressed in terms of $H_{\tau 2}$, the scale height at r_2, the level at which $\tau = 1$. The published version of the paper gives $\tau(r)$ in terms of $H_{\tau 1}$, the scale height at r_1, the level at the top of the haze. To convert from one version to another, note that $H_{\tau 1} = H_{\tau 2}(r_2/r_1)^2$.

performed for the KAO and for the Charters Towers immersion and emersion curves separately. The Hobart, Mt. John, and Black Birch curves do not reach the Pluto-alone level and, except for possibly Black Birch, do not even reach the haze layer. For these lightcurves, we held the three haze parameters constant at the values determined from the KAO fit; we also held the Pluto-alone level constant either at a predetermined value based on Pluto's rotational lightcurve and the bandpass of the observations or, where possible, on resolved observations of Pluto and P8 before or after the occultation at that site. The remaining four parameters—the two atmospheric ones, the Pluto + Star baseline, and the X shift—were then determined from the least-squares solutions. The Toowoomba and Mt. Tamborine data sets were too noisy to fit separately. For these two lightcurves, we took a straight line fit to the Pluto + Star and Pluto-alone levels for both baselines. See Table IV for results of these preliminary solutions. In the overall global fit, the baselines determined in this way were used and not allowed to vary.

In order to do a least-squares fit to the data, one needs to be able to compare the observed flux with the calculated flux in Eq. (1). But, the observed flux is known as a function of time and the calculated flux is determined as a function of the radial distance from Pluto. We have shown earlier how to convert the observed flux into a function of X in the shadow plane. Note that for each observatory we have a fixed impact parameter $Y_{\rm imp}$ from the astrometric solution and that $X = \sqrt{\rho^2 + Y_{\rm imp}^2}$ so that we can find the observed flux as a function of ρ. Unfortunately, we cannot derive a simple conversion from ρ to r since $\rho = r + D\theta(r)$. Thus an iterative scheme must be used to convert the observed flux as a function of ρ to an observed flux as a function of r. Our approach was to choose two values of r separated by 5 km such that their corresponding values of ρ bracket the desired value. We then employed a binary search in order to find the value of r which corresponded to the desired value of ρ. Next, the derivatives of the calculated flux (as a function of r) with respect to the unknown parameters were taken numerically except for the derivatives with respect to the individual X shifts which can be found analytically.

Three global solutions with three different weighting schemes were calculated (see Table V). In the first solution, each data set was weighted as the square of the S/N ratio. In the second solution, each data set was weighted as the S/N ratio. In the third solution, we arbitrarily assigned a weight of 1.0 to the "best" data set, a weight of 0.5 to the "good" data sets, and a weight of 0.1 to the other data sets, except for Auckland, which again was given zero weight. Note in Table V that the choice of weighting scheme actually made little difference in the results. Because the S/N squared weighting scheme is theoretically most appropriate, we selected solution 1 for further study. In particular, we wish to assess its sensitivity to parameters other than the weighting scheme and thereby determine more realistic estimates of the uncertainties in the derived results.

Selected parameters from this solution are repeated in the column labeled "Solution 1" in Table VI; and corresponding model lightcurves are shown fitted to the data in Fig. 5 and the two left-hand panels of Fig. 6. The second solution in Table VI is also weighted inversely as the square of the S/N ratio, except that the center of the ground track on the fundamental plane was moved north by an amount equal to the 1σ error in the adopted astrometric solution (i.e., a ground track shift of about 6 km). The third solution in Table VI is also weighted inversely as the square of the S/N ratio, but here we artificially moved the KAO south by 15 km, recomputed the astrometric solution and the atmospheric solution. The three solutions are quite similar. The resulting predicted Black Birch and Mt. John lightcurves for solutions 2 and 3 are shown plotted against the observations in the center and right-hand panels of Fig. 6, respectively. Solution 2 gives a slightly better fit to the Black Birch data than the "preferred" fit in the left-hand panels because moving Pluto north makes the Black Birch chord dip less into the haze layer. However, in this case the Mt. John data fit slightly worse than for the preferred solution. Solution 3 does not give results significantly different from those of the "preferred" solution.

The uncertainties quoted in Table VI are formal uncertainties in the least-squares solution and do not reflect the true uncertainty in the radii determined. A better estimate of the true uncertainties is obtained by comparing the results from the different solutions. We have listed in Table VII the final adopted results from this study along with more realistic estimates of the uncertainties.

V. DISCUSSION

The results from the 9 June 1988 occultation in Table VII place the "haze top" at 1214 ± 5 km, and the distance from the center of the planet at which the light from P8 was diminished by $1/e$ (optical depth unity) at 1200 ± 5 km. Moreover, careful analysis of the KAO lightcurve places the distance from the center of the planet at which the light from P8 was completely extinguished near 1180 km. All these values conflict with the radius of Pluto of 1151 ± 20 km derived by Tholen and Buie (1990)[3] from observations of the Pluto/Charon mutual events.

The radius derived from the mutual events, of course,

[3] Tholen and Buie quote an uncertainty of ±6 km, but including the uncertainty in Charon's semimajor axis increases this value to ±20 km.

TABLE V
Global Solutions to Data

	Solution 1		Solution 2		Solution 3	
	Derived value	Weight	Derived value	Weight	Derived value	Weight
λ_0	22.63 ± 0.23		22.86 ± 0.30		22.84 ± 0.30	
$\nu_0 \times (10^{-10})$	8.14 ± 0.11		7.54 ± 0.16		7.50 ± 0.16	
Haze top radius (km)	1213.87 ± 0.31		1213.42 ± 0.47		1213.45 ± 0.49	
$\tau = 1$ Radius	1200.25 ± 0.34		1197.27 ± 0.50		1196.98 ± 0.52	
Haze scale height (km)	27.3 ± 1.7		29.6 ± 2.2		30.6 ± 2.3	
KAO shift (km)	−6.12 ± 0.70	1.0	−4.18 ± 0.84	1.0	−4.58 ± 0.97	1.0
Charters Towers shift (km)	−12.45 ± 1.43	0.1	−9.80 ± 1.36	0.31	−9.90 ± 1.31	0.5
Black Birch shift (km)	−13.31 ± 7.43	0.06	−10.31 ± 9.76	0.25	−10.28 ± 8.47	0.5
Hobart shift (km)	18.90 ± 15.33	0.04	18.73 ± 12.21	0.20	18.73 ± 9.48	0.5
Mt. John shift (km)	−7.46 ± 26.23	0.08	−7.43 ± 25.39	0.29	−7.43 ± 23.73	0.5
Mt. Tamborine shift (km)	19.70 ± 15.70	0.003	19.85 ± 30.86	0.05	19.85 ± 26.77	0.1
Toowoomba shift (km)	42.79 ± 17.72	0.006	36.12 ± 5.48	0.08	36.34 ± 6.02	0.1
Auckland shift (km)	46.53 ± 174.64	0	45.71 ± 289.11	0	45.73 ± 354.77	0

Note. Solution 1, weight inversely as the 1-sec signal-to-noise squared. Solution 2, weight inversely as the 1-sec signal-to-noise. Solution 3, weight according to value judgment of data.

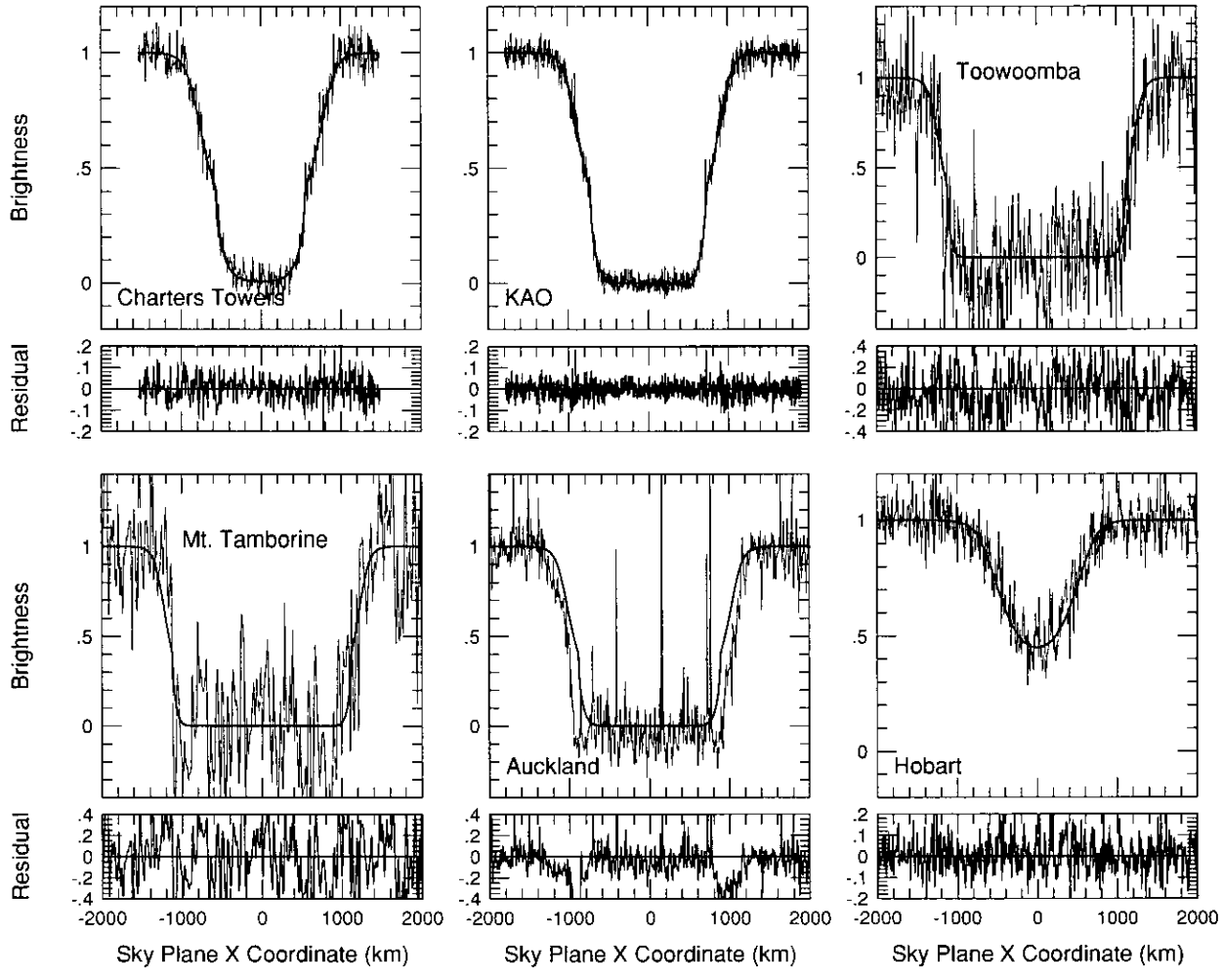

FIG. 5 Model lightcurves fitted to the data according to the preferred solution.

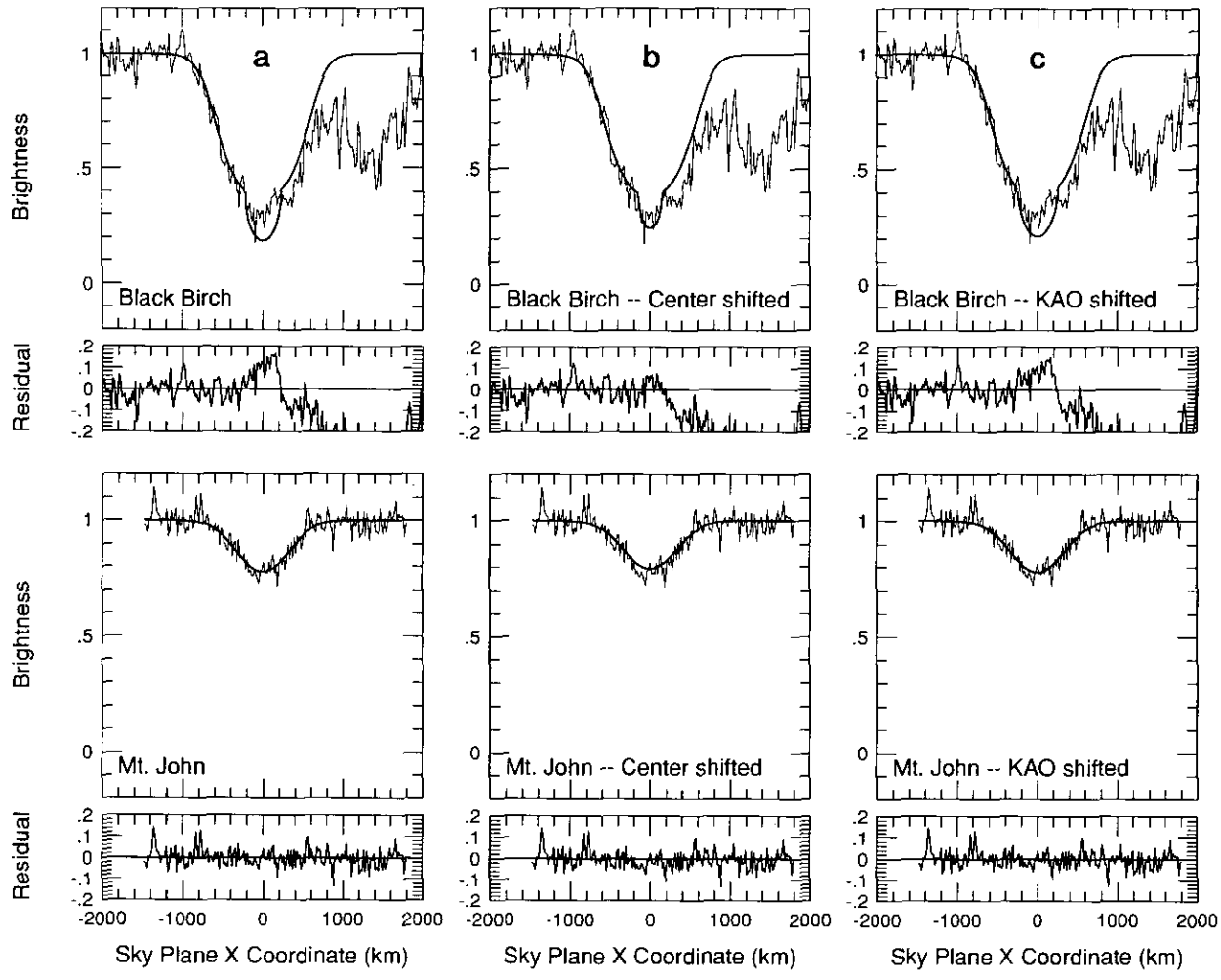

FIG. 6. Model lightcurves fitted to the Mt. John and Black Birch data using (a) the preferred solution; (b) assuming that the ground track was 6 km north of the nominal position; and (c) with the KAO shifted 15 km south of its nominal position.

pertains to the visible limb of the planet. Under the thermal gradient model, the visible limb coincides with Pluto's solid surface. While observations of the 9 June occultation did not probe all the way to the solid surface, Hubbard *et al.* (1990) have shown that the thermal gradient model, in order to fit the observed occultation lightcurves, requires a very steep decrease in temperature beginning at a value near 106 K in the isothermal region above the step in the lightcurve (Yelle and Lunine 1989). The magnitude of the thermal gradient quickly approaches 10° K/km. We do not know the exact temperature of the surface of Pluto. As discussed by Elliot and Young (1992), published values fall within range from 31 to 59 K. However, the upper third of this span is ruled out by vapor pressure considerations. Assuming the more restricted range of possible surface temperatures, a first-order fit of a thermal gradient model to the KAO data indicated that the solid surface of the planet falls at 1195 ± 5 km.

TABLE VI
Impact of Known Uncertainties on Preferred Solution

	Solution 1 (preferred)	Solution 2[a] Pluto shifted 1σ N	Solution 3[a] KAO shifted 15 km S
λ_0	22.27 ± 0.23	22.08 ± 0.23	22.13 ± 0.24
$\nu_0 \times 10^{-10}$	8.14 ± 0.11	8.23 ± 0.13	7.85 ± 0.13
Haze top (km)	1213.87 ± 0.31	1210.67 ± 0.32	1213.34 ± 0.33
τ = 1 (km)	1200.25 ± 0.34	1198.47 ± 0.38	1194.97 ± 0.45
Haze scale height (km)	27.3 ± 1.7	31.7 ± 2.4	20.3 ± 1.3

Note. Solution 1, preferred solution taken from column 1 of Table V.
[a] Solutions 2 and 3 result from recomputing impact parameters and refitting the global solution after applying the indicated shifts in the position of Pluto and the KAO, respectively.

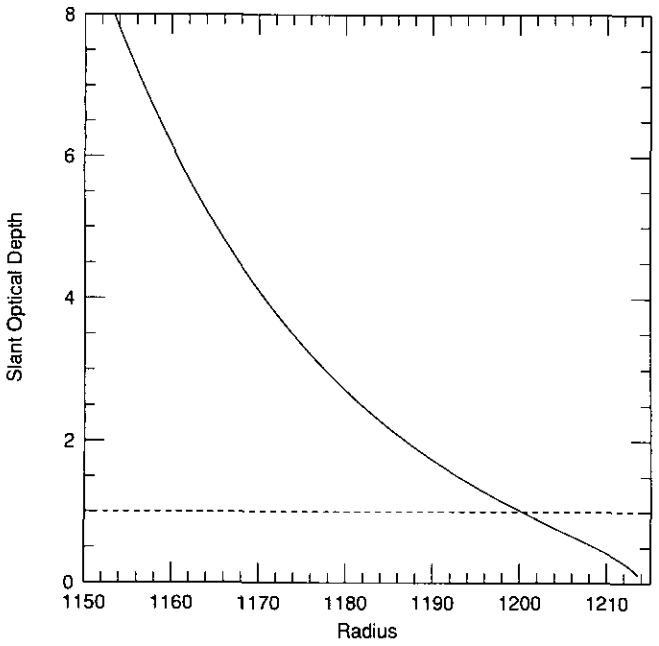

FIG. 7. Slant optical depth as a function of radius for the preferred solution's haze parameters. The dashed line denotes $\tau = 1$.

Under the haze model, the limb would be less sharp than in the case of a clear atmosphere. The slant optical thickness of the haze at the limb is shown as a function of radius in Fig. 7. The visible limb as determined from the mutual events, would be expected to correspond to a τ in the range of 1 to 2, or a radius between 1187 and 1200 km. The solid surface of the planet would necessarily be below about 1180 km radius, if the haze model is correct, because if the radius were larger, another sharp step near the bottom of the lightcurve would have been detectable in the KAO, Charters Towers, and Auckland lightcurves (at Toowoomba and Mount Tamborine this step would have been lost in the noise).

The source of the discrepancy in the values of the radius derived from the mutual events and from the stellar occultation is not immediately evident. In our analysis of the stellar occultation data, the position of the center of Pluto's shadow relative to the observing sites is dependent primarily on the observations from Charters Towers, KAO, Black Birch, Hobart, and Mt. John, and on the assumption of a symmetric atmosphere above the "haze top." The position of the visible limb, then, results from the observed height in the atmosphere at which the break in the lightcurve was observed at Charters Towers and at the KAO and from the shape of the lightcurve below that point. All these observations are mutually consistent and yield a very well-defined value for the radius of the limb. The observations which agree less well—those from Toowoomba, Mt. Tamborine, and Auckland—are also those of lower signal-to-noise ratio, poorer mutual consistency (Toowoomba and Mt. Tamborine), and apparent timing difficulties (Auckland). Moreover, we have demonstrated in Table VI that the known uncertainties in the position of the KAO and in the position of the center line of the occultation ground track impact the derived radius of the limb by much less than is needed to account for the difference between our result and that of Tholen and Buie.

Determination of the radii of Pluto and Charon from observations of the mutual events requires knowledge of the semimajor axis of Charon's orbit since that parameter plus the known orbital period establishes the relationship between the observed duration of the mutual events and the sizes of the two bodies. Tholen and Buie adopted the value for the semimajor axis of 19,640 ± 320 km as determined from speckle interferometry by Beletic *et al.* (1989). If the actual radius of the orbit is about 2.5σ larger than the Beletic et al. value, the radius of Pluto derived from the mutual events would then agree with the occultation result.

Another possible cause of the difference in the derived radii is the absence of limb darkening in the Tholen and Buie model. If significant limb darkening is in fact present, it is very likely that their modeling of the mutual event lightcurves has yielded an underestimate of Pluto's radius. Testing of this possibility would seem to be worthwhile, particularly if further observations confirm the speckle result for the semimajor axis of Charon's orbit. In fact, using a different mutual event data set, but allowing the limb darkening of Pluto and Charon to be free parameters, E. Young (1992) has found radii of 1191 ± 20 km for Pluto and 642 ± 11 km for Charon. These values are consistent with the radius of Pluto derived in this paper and with the lower limit on Charon's radius of 601.5 km derived by Elliot and Young (1991).

Tholen and Buie have computed the mean density of

TABLE VII
Occultation Results

	Haze model	Thermal gradient model
Haze top radius	1214 ± 5 km	—
Radius at $\tau = 1$	1200 ± 5 km	—
Radius of visible limb	1187 – 1200 km	1195 ± 5 km
Radius of solid surface	<1180 ± 5 km	1195 ± 5 km
System density[a]	≥1.8 ± 0.1 gm/cm^3	1.78 ± 0.09 gm/cm^3
Density of Pluto[b]	≥1.9 gm/cm^3	1.9 gm/cm^3
Density of Charon[b]	1.1 gm/cm^3	1.1 gm/cm^3

[a] Assuming masses determined by Null *et al.* (1992) and radii quoted in this paper.

[b] Assuming system mass determined by Beletic *et al.* (1989) and radii quoted in this paper.

the Pluto/Charon system to be 2.03 ± 0.04 gm/cm^3, assuming the radii for the planet and satellite and the orbital period derived from their model. If the difference between the mutual event and occultation results for Pluto's radius is due entirely to an error in the semimajor axis, the system density remains unchanged. Both the system mass and the volume of the two bodies vary in proportion to the semimajor axis cubed. If, on the other hand, the Beletic *et al.* value for the semimajor axis is correct and the discrepancy is due to some other factor such as limb darkening, then Pluto's density could differ from the value derived by Tholen and Buie. For example, if the thermal gradient model is correct, the solid surface of Pluto is near 1195 ± 5 km and the system density drops to 1.78 ± 0.09 gm/cm^3 assuming that Charon has the radius of 642 ± 11 km derived by Young (1992) and the same density as Pluto. On the other hand, if the haze model is correct, the occultation data tell us only that the solid surface lies below 1180 km and we can set only a lower limit on the density.

Recently, Null *et al.* (1992) have determined values of 2.1 and 1.4 gm/cm^3 for the densities of Pluto and Charon, respectively, from HST observations of the "wobble" of the two bodies in their mutual orbit. These densities were derived under the assumption of the Pluto and Charon radii of 1151 and 593 km. From our discussion above, we would interpret the Null *et al.* results with different radii: if the thermal gradient model is correct, then the density of Pluto is 1.9 gm/cm^3 and that of Charon is 1.1 gm/cm^3. If the haze model is correct, 1.9 gm/cm^3 is a lower limit on Pluto's density.

ELL considered a number of approaches to setting a lower limit on Pluto's radius assuming that the step in the occultation lightcurve is due to a haze layer. Perhaps the most compelling of these is based on the fact that Pluto has shown since 1954 (Walker and Hardie 1955) a rotational lightcurve whose amplitude has varied between 0.12 and 0.30 mag in *B* (Buie and Tholen 1989). Consequently, albedo features on the planet's surface are not wholly obscured by the haze, at least away from the limb. ELL estimated that the vertical optical depth of the haze could not be more than 0.5 to 1.0 for the lightcurve amplitude to be as large as is observed. The corresponding radii for the bottom of the haze layer from our analysis are 1152 and 1136 km, respectively. However, even if the solid surface falls somewhere in this range (or if the haze is detached and the radius of Pluto is below 1136 km), our modeling indicates that evidence of the solid surface would not be detectable in the existing occultation lightcurves.

In our opinion, evidence exists that neither a pure haze nor a pure thermal gradient model is correct. Yelle and Lunine (1989) have predicted that, if methane is present, the isothermal region of Pluto's atmosphere will have a temperature near 106 K. This temperature, together with the thermal scale height from the occultation, requires that the mean molecular weight of the atmospheric gases be close to 25 amu which, in turn, requires that a molecule heavier than methane be present. Yelle and Lunine suggested on cosmochemical grounds that CO and N_2 are the most likely candidates. Owen *et al.* (1992) subsequently discovered absorption features of solid forms of both species and stated that each would be more abundant than CH_4 in Pluto's atmosphere. Consequently, Yelle and Lunine's prediction of a heavier gas is confirmed observationally; and a thermal gradient must be present. On the other hand, a pure thermal gradient model predicts that in the stellar occultation, the light from P8 would not have been completely extinguished even at mid-event. In fact, the well-calibrated observations from the KAO show that it was. Some amount of haze in the atmosphere of Pluto could explain this observed characteristic of the lightcurve. Given the hazy atmospheres of Titan and particularly of Triton (e.g., Rages and Pollack 1992), haze on Pluto would not be unexpected.

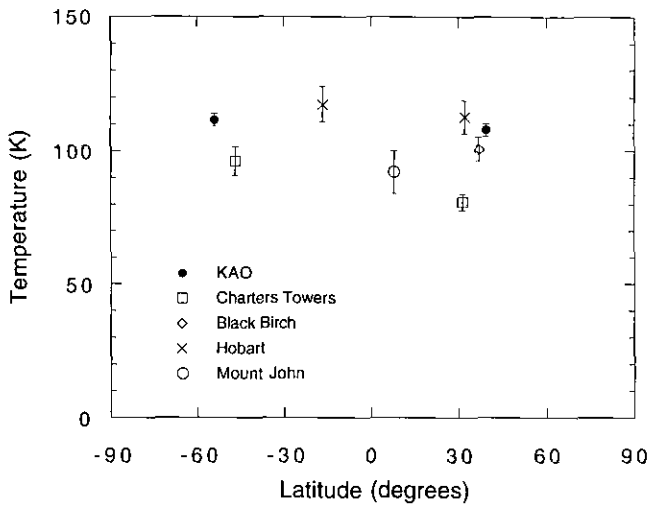

FIG. 8. Atmospheric temperature versus latitude for Pluto. Temperatures and error bars have been derived from an isothermal model for the lightcurve of each station (see text). The temperature scatter is no greater than ±15° K from an isothermal model, and no systematic trends with latitude are evident.

Another question which we hoped to address based on the occultation observations is that of the global uniformity of the structure of Pluto's atmosphere. In Fig. 8, we have plotted the atmospheric temperature as a function of latitude on Pluto, derived from the values of λ_0 and ν_0 given in Table IV (assuming a mean molecular weight of 28). Each latitude is that directly below the corresponding occultation point on Pluto's limb for the observing station, and the errors in the temperatures have been derived from propagating the formal errors in λ_0 and ν_0. The measure-

ments span a large latitude range from −60° to +60° and would seem to scatter by an amount greater than could be explained by their error bars. However, we believe this scatter could well be explained by the formal errors being underestimates of the real errors, and we prefer to interpret the scatter as an upper limit for atmospheric temperature variation on Pluto. Certainly there appears to be no systematic trend with latitude.

One would also like to know whether the haze layer (and/or thermal gradient) is planetwide in extent and uniform in character. Unfortunately, the available observations do not allow a definitive answer to this question. The observations from Charters Towers and the KAO sampled the atmosphere in both the northern and southern hemispheres of Pluto and yielded mutually consistent results (see Figs. 3 and 9). Both were on the sunrise limb. Toowoomba and Mt. Tamborine probed the atmosphere near the poles of the planet. However, the signal-to-noise ratio of these observations is such that the existence of the sharp step in the lightcurves could be argued. We believe it is clearly seen in the Toowoomba data and, as is seen in Fig. 5, the model lightcurve we have derived fits well. The fit of the model to the Mt. Tamborine observations, on the other hand, is not convincing, as that lightcurve is decidely asymmetric. Since both sites sampled the same chord across Pluto, the differences must be in the observations and not on the planet. We note that the Toowoomba observations have a signal-to-noise ratio twice that of those from Mt. Tamborine, and we accordingly give them higher weight.

The most convincing evidence of a possible departure from global uniformity in atmospheric structure is seen in the Auckland data. In Fig. 2, the Auckland observations clearly show the step in the lightcurve on immersion. However, the character of the lightcurve on emersion is very different with the step being much shorter than on immersion. While we have discussed the timing problems of the Auckland data earlier in the paper, we see no obvious way that those could have produced the observed asymmetry. Therefore, we must remain open to the possibility that this asymmetry is due to a difference in Pluto's atmospheric structure at the immersion and emersion locations.

Black Birch is the only other site from which the observations probed deeply enough into the atmosphere to reach the haze or thermal gradient region. As we have shown in Fig. 5, to within the uncertainties in the position of the groundtrack and the location of the KAO, the Black Birch immersion observations are consistent with the results from Charters Towers and the KAO. Black Birch probed the same latitude in the planet's northern hemisphere as did Charters Towers and KAO, but at the sunset, rather than sunrise, limb.

The 9 June 1988 occultation of P8 by Pluto has taught us much about the Solar System's ninth planet. It also has taught valuable lessons to be borne in mind in planning and executing observations of future Pluto occultations. In particular, the importance of accurate timing and high photometric quality cannot be overemphasized. Greater uniformity in the passbands used for observations at different sites and an accurate determination of the relative brightness of Pluto and the target star at each site would be extremely valuable.

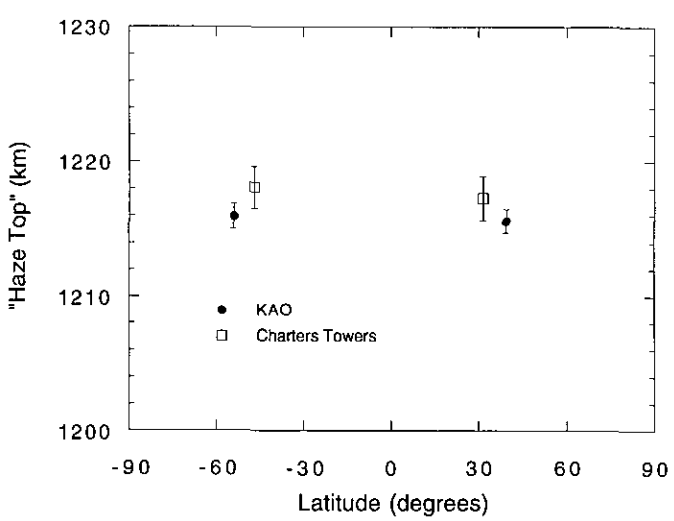

FIG. 9. Haze top versus latitude for KAO and Charters Towers. For these limited data (four points), whatever atmospheric structure that causes the break in the lightcurve—haze or the onset of a steep thermal gradient—occurs at the same altitude.

VI. CONCLUSIONS

An analysis of all observations of the 9 June 1988 occultation of P8 by Pluto has shown that an isothermal model with a haze layer below 1214 ± 5 km is consistent with all of the higher quality observations. A haze-free model in which a steep near-surface thermal gradient is overlaid by an isothermal region also fits the observations, except for its inability to produce total quenching of the light from P8 as was observed by the KAO. The haze model, when fitted to the stellar occultation data, predicts that the visible limb of the planet falls at a radius between 1185 and 1200 km. If the atmosphere is clear, the visible limb corresponds to the solid surface of Pluto and falls at 1195 ± 5 km. If the haze model is correct, the solid surface falls below 1180 km, but the occultation data alone cannot set a lower limit on this value. In either case, the stellar occultation observations reported in this paper require that the radius of the visible limb of the planet be larger than that derived from observations of the extensive series of Pluto/Charon mutual events by Tholen and Buie (1989). Similarly, adoption of the occultation radius leads

to a value of Pluto's density near 1.9 gm/cm^3, assuming a clear atmosphere. If significant haze is present, this value is a lower limit.

ACKNOWLEDGMENTS

We thank the staff of the U.S. Naval Observatory Flagstaff Station for taking the plates upon which the predictions of the 9 June 1988 occultation were based. Without their work, accurate prediction of this event would not have been possible. Additionally, we are grateful to Francois Roques, Larry Lebofsky, and David Tholen for constructive comments based on an earlier version of this paper. This research was supported at Lowell Observatory by NASA Grants NAGW-1912 and NSG-7603 and at MIT by NASA Grants NSG-7526 and NAG 2-475 and NSF Grant AST 8519518.

REFERENCES

BELETIC, J. W., R. M. GOODY, AND D. J. THOLEN 1989. Orbital elements of Charon from speckle interferometry. *Icarus* **79,** 38–46.

BOSH, A. S., J. L. ELLIOT, S. E. KRUSE, R. L. BARON, E. W. DUNHAM, AND L. M. FRENCH 1986. Signal-to-noise ratios for possible stellar occultations by Pluto. *Icarus* **66,** 556–560.

BUIE, M. W., AND D. J. THOLEN 1989. The surface albedo distribution of Pluto. *Icarus* **79,** 23–37.

CRUIKSHANK, D. P. 1987. Pluto, Charon, and Triton: A review of their physical parameters, atmospheres, and surfaces. *Bull. Am. Astron. Soc.* **19,** 858.

ELLIOT, J. L., E. W. DUNHAM, A. S. BOSH, S. M. SLIVAN, L. A. YOUNG, L. H. WASSERMAN, AND R. L. MILLIS 1989. Pluto's atmosphere. *Icarus* **77,** 148–170.

ELLIOT, J. L., AND L. A. YOUNG 1991. Limits on the radius and possible atmosphere of Charon from its 1980 stellar occultation. *Icarus* **89,** 244–254.

ELLIOT, J. L., AND L. A. YOUNG 1992. Analysis of stellar occultation data for planetary atmospheres. I. Model fitting, with application to Pluto. *Astron. J.* **103,** 991–1015.

ESHLEMAN, V. R. 1989. Pluto's atmosphere: Models based on refraction, inversion, and vapor–pressure equilibrium. *Icarus* **80,** 439–443.

HUBBARD, W. B., D. M. HUNTEN, S. W. DIETERS, K. M. HILL, AND R. D. WATSON 1988. Occultation evidence for an atmosphere on Pluto. *Nature* **336,** 452–454.

HUBBARD, W. B., R. V. YELLE, AND J. I. LUNINE 1990. Nonisothermal Pluto atmosphere models. *Icarus* **84,** 1–11.

MILLIS, R. L., L. H. WASSERMAN, O. G. FRANZ, R. A. NYE, A. C. GILMORE, P. M. KILMARTIN, W. H. ALLEN, R. D. WATSON, S. W. DIETERS, K. M. HILL, A. B. GILES, G. BLOW, J. PRIESTLY, W. S. G. WALKER, B. K. MARINO, D. G. DIX, A. PAGE, H. D. KENNEDY, J. L. ELLIOT, E. DUNHAM, A. S. BOSH, L. A. YOUNG, S. M. SLIVAN, AND A. R. KLEMOLA 1988. Observations of the 9 June 1988 occultation by Pluto. *Bull. Am. Astron. Soc.* **20,** 806.

MINK, D. J., AND A. KLEMOLA 1985. Predicted occultations by Uranus, Neptune, and Pluto: 1985–1990. *Astron. J.* **90,** 1894–1899.

NULL, G. W., W. M. OWEN JR., AND S. P. SYNNOTT 1992. Masses and densities of Pluto and Charon determined from HST observations. *Bull. Am. Astron. Soc.* **24,** 962.

OWEN, T., T. GEBALLE, C. DE BERGH, L. YOUNG, J. ELLIOT, D. CRUIKSHANK, T. ROUSH, B. SCHMITT, AND R. H. BROWN 1992. Detection of nitrogen and carbon monoxide on the surface of Pluto. *Bull. Am. Astron. Soc.* **24,** 961.

RAGES, K., AND J. B. POLLACK 1992. Voyager imaging of Triton's clouds and hazes. *Icarus* **99,** 289–301.

SMART, W. M. 1960. *Textbook in Spherical Astronomy,* 4th ed. Cambridge Univ. Press, London.

THOLEN, D. J., AND M. W. BRUIE 1989. Further analysis of the Pluto–Charon mutual event observations—1989. *Bull. Am. Astron. Soc.* **21,** 981–982.

THOLEN, D. J., AND M. W. BUIE 1990. Further analysis of the Pluto–Charon mutual event observations—1990. *Bull. Am. Astron. Soc.* **22,** 1129.

TRAFTON, L., AND S. A. STERN 1983. On the global distribution of Pluto's atmosphere. *Astrophys. J.* **267,** 872–881.

WALKER, M. F., AND R. HARDIE 1955. A photometric determination of the rotational period of Pluto. *Publ. Astron. Soc. Pac.* **67,** 224–231.

WASSERMAN, L. H., R. L. MILLIS, O. G. FRANZ, A. R. KLEMOLA, AND C. C. DAHN 1988. Precise astrometry of the Pluto/Charon system. *Bull. Am. Astron. Soc.* **20,** 806.

YELLE, R. V., AND J. I. LUNINE 1989. Evidence for a molecule heavier than methane in the atmosphere of Pluto. *Nature* **339,** 288–290.

YOUNG, E. F. 1992. *An Albedo Map and Frost Model of Pluto.* Ph.D. thesis, Massachusetts Institute of Technology, Cambridge, MA.